

STRUCTURE-INFORMED BOUNDS ON THE KRONECKER RANK OF BLOCK-STRUCTURED MATRICES

ALLISON FULLER*, MALENA I. ESPAÑOL*, AND MISHA E. KILMER†

Abstract. We derive theoretical bounds on the Kronecker rank of block-structured matrices that possess both inner and outer structure. Building on the matrix-to-tensor and tensor-to-matrix framework of Kilmer and Saibaba (*SIAM J. Matrix Anal. Appl.*, 2022), we show that the Kronecker rank of a matrix \mathbf{A} equals the dimension of the span of its distinct blocks (the *inner blockspan*), and equals as well the dimension of the corresponding span for a permuted matrix \mathbf{B} whose inner and outer structures are interchanged. We give two proofs of this equality: one via a direct dimension argument, and one via an explicit isomorphism between the outer blockspan of \mathbf{A} and the column space of the second-mode unfolding of the associated tensor. These results yield nested containments that translate structural information, such as Toeplitz, Hankel, banded, or sparse patterns, into computable upper bounds on the Kronecker rank. We also establish a duality between element-level sparsity in \mathbf{A} and block-level sparsity in \mathbf{B} . Numerical experiments confirm the theory across several classes of structured matrices and, for two sparse matrices drawn from the SuiteSparse collection, provide a structural explanation for observed singular value decay.

1. Introduction. Large, structured matrices arise in many applications, including linear inverse problems and the discretization of ordinary and partial differential equations. Their size often makes storage and computation prohibitively expensive. One effective way to mitigate these costs is to express such matrices as a sum of Kronecker products, thereby exploiting Kronecker structure to reduce storage requirements and accelerate matrix-vector products.

The classical approach to writing a matrix as a sum of Kronecker products originated with Van Loan and Pitsianis [15], and was later expanded by Pitsianis [19]. They showed that any matrix $\mathbf{A} \in \mathbb{R}^{(\ell m) \times (qn)}$ admits the exact representation

$$\mathbf{A} = \sum_{j=1}^r \mathbf{C}_j \otimes \mathbf{D}_j,$$

where $\mathbf{C}_j \in \mathbb{R}^{\ell \times q}$ and $\mathbf{D}_j \in \mathbb{R}^{m \times n}$ are obtained from singular vectors of a reshuffled version of \mathbf{A} . The integer r is the *Kronecker rank* of \mathbf{A} . Despite its strong theoretical guarantees, this approach is often impractical at large scale, as it requires computing the singular value decomposition of a matrix comparable in size to \mathbf{A} .

Motivated by these limitations, we focus on a structured subclass of matrices for which more scalable Kronecker-based representations may be obtained, namely, large *block-structured matrices*. We use the term *block matrix* to denote a matrix partitioned into submatrices, called *blocks*, and assume throughout that all blocks are of equal size. For example, a matrix $\mathbf{A} \in \mathbb{R}^{(\ell m) \times (qn)}$ may be viewed as an $\ell \times q$ block matrix with ℓq blocks arranged in an ℓ -by- q grid, each of size $m \times n$. We adopt a broad notion of *structure*, encompassing both pattern-based structure (e.g., Toeplitz or Hankel matrices) and sparsity-based structure (e.g., diagonal or banded matrices). A *block-structured matrix* is therefore a block matrix whose blocks exhibit such properties.

Kilmer and Saibaba [12] introduced a tensor-based framework tailored to such block-structured matrices. Their method assembles the distinct blocks of \mathbf{A} into a

*School of Mathematical and Statistical Sciences, Arizona State University, Tempe, AZ, United States (tjfuller@asu.edu, mespanol@asu.edu).

†Department of Mathematics, Tufts University, Medford, MA, United States (misha.kilmer@tufts.edu)

tensor and approximates it using a Tucker decomposition; when mapped back to the matrix domain, this yields a sum of Kronecker products whose length is determined by the second-mode rank of the tensor. Several examples in that work show that highly structured block matrices can be approximated to within machine precision using only a small number of Kronecker terms. This empirical observation raises a natural question: can one determine *a priori* bounds on the Kronecker rank from the structural properties of the matrix alone?

In this paper, we answer this question by deriving exact characterizations and computable upper bounds on the Kronecker rank of matrices with both outer and inner block structures. Our approach combines the invertible matrix-to-tensor mapping of [12] with subspace dimension arguments defined by the block layout, the internal structure of the blocks, and a stride permutation of \mathbf{A} . The main contributions are as follows.

- We show that the Kronecker rank of \mathbf{A} equals the dimension of the linear span of its distinct blocks (Theorem 4.1).
- We prove that this dimension is invariant under the permutation that interchanges inner and outer structure, via both a direct dimension argument (Theorem 4.3) and an explicit isomorphism with the column space of the second-mode unfolding (Lemma 4.4).
- We establish nested containments linking structural subspaces to the Kronecker rank, yielding computable upper bounds from Toeplitz, Hankel, banded, and related structure (Corollary 5.1).
- We derive a sparsity-based bound and a duality between element-level sparsity in \mathbf{A} and block-level sparsity in the permuted matrix \mathbf{B} (Theorems 5.4 and 5.6).
- We show, through numerical experiments, that these structural bounds give tight upper bounds that explain the singular value decay observed in [12] for specific matrices from the SuiteSparse collection [2].

Prior work on Kronecker rank has focused primarily on matrices whose entries are given by smooth functions [6, 20]. In application-driven settings such as image deblurring, related work has examined representations of structured operators as sums of structured Kronecker products [8, 9, 11, 17, 18]. In contrast, our results are structure-driven and deterministic, and apply to a broad class of block-structured matrices.

Notation and terminology. Scalars are italicized lowercase (a), vectors bold lowercase (\mathbf{a}), index sets italicized uppercase (A), matrices bold uppercase (\mathbf{A}), tensors of order three or higher calligraphic uppercase (\mathcal{A}), and subspaces of matrices script uppercase (\mathcal{A}). We write $[n] = \{1, \dots, n\}$.

A matrix that is symmetric across its main antidiagonal is *persymmetric*. We write $\mathbf{A}^{(\gamma, \delta)}$ for the block of \mathbf{A} in block-position (γ, δ) . If $\ell = q$, we say that a matrix is *block-symmetric* if $\mathbf{A}^{(\gamma, \delta)} = \mathbf{A}^{(\delta, \gamma)}$ for all (γ, δ) with $\gamma, \delta \in [\ell]$, and analogously, a matrix is *block-persymmetric* if $\mathbf{A}^{(\gamma, \delta)} = \mathbf{A}^{(\ell - \delta + 1, \ell - \gamma + 1)}$.

Organization. Section 2 reviews the Kronecker product, tensor basics, the Tucker decomposition, and the matrix-to-tensor framework of [12]. Section 3 defines the sets and subspaces used throughout. Section 4 establishes the connection between blockspans and Kronecker rank, and gives both proofs of the dimension equality. Section 5 derives structure-informed and sparsity-informed upper bounds. Section 6 presents numerical experiments. Section 7 offers conclusions and directions for future work.

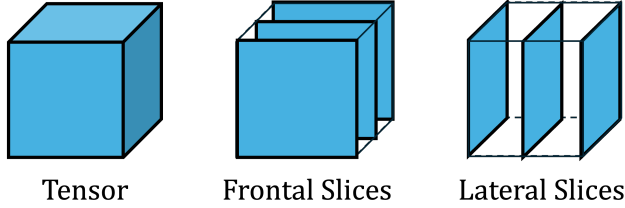


Fig. 2.1: Illustration of a 3-way tensor and two types of slices.

2. Background.

2.1. The Kronecker Product. The Kronecker product of $\mathbf{C} \in \mathbb{R}^{\ell \times q}$ and $\mathbf{D} \in \mathbb{R}^{m \times n}$ is the $(\ell m) \times (qn)$ matrix

$$\mathbf{C} \otimes \mathbf{D} = \begin{bmatrix} c_{11}\mathbf{D} & \cdots & c_{1q}\mathbf{D} \\ \vdots & \ddots & \vdots \\ c_{\ell 1}\mathbf{D} & \cdots & c_{\ell q}\mathbf{D} \end{bmatrix}.$$

The following properties will be used throughout [1, 5, 14, 16]:

1. $(\mathbf{C} \otimes \mathbf{D})^\top = \mathbf{C}^\top \otimes \mathbf{D}^\top$.
2. $\mathbf{C} \otimes (\mathbf{D} + \mathbf{E}) = (\mathbf{C} \otimes \mathbf{D}) + (\mathbf{C} \otimes \mathbf{E})$.
3. $(\mathbf{C} \otimes \mathbf{D})\mathbf{x} = \text{vec}(\mathbf{D}\mathbf{X}\mathbf{C}^\top)$, where $\mathbf{x} = \text{vec}(\mathbf{X})$ and $\text{vec}(\cdot)$ stacks columns.
4. There exist permutation matrices \mathbf{P} and \mathbf{Q} such that

$$\mathbf{P}(\mathbf{C} \otimes \mathbf{D})\mathbf{Q}^\top = \mathbf{D} \otimes \mathbf{C},$$

where $\mathbf{P} = \mathbf{S}_{\ell, m}$, $\mathbf{Q} = \mathbf{S}_{q, n}$, and

$$(2.1) \quad \mathbf{S}_{a,b} = \begin{bmatrix} [\mathbf{I}_s]_{1:b:s,:} \\ [\mathbf{I}_s]_{2:b:s,:} \\ \vdots \\ [\mathbf{I}_s]_{b:b:s,:} \end{bmatrix}, \quad s = ab.$$

2.2. Tensor Basics. We use *tensor* to denote a multiway array; unless otherwise stated, all tensors are third-order. By fixing all but one index of \mathcal{A} , we obtain *fibers*; by fixing all but two indices, we obtain two-dimensional *slices* [13] (see Figure 2.1). We write $\mathbf{A}^{[k]} = \mathcal{A}_{:, :, k}$ for the k th frontal slice and $\vec{\mathcal{A}}_j = \mathcal{A}_{:, j, :}$ for the j th lateral slice. The operators $\text{twist}(\cdot): \mathbb{R}^{m \times p \times 1} \rightarrow \mathbb{R}^{m \times 1 \times p}$ and $\text{squeeze}(\cdot): \mathbb{R}^{m \times 1 \times p} \rightarrow \mathbb{R}^{m \times p \times 1}$ reorient frontal slices as lateral slices and vice versa [10]. See Figure 2.2 for a visualization of these operators.

The *mode- i unfolding* $\mathbf{A}_{(i)}$ is formed by arranging mode- i fibers as columns. For $\mathcal{A} \in \mathbb{R}^{m \times p \times n}$:

$$\begin{aligned} \mathbf{A}_{(1)} &= [\mathbf{A}^{[1]}, \mathbf{A}^{[2]}, \dots, \mathbf{A}^{[n]}] \in \mathbb{R}^{m \times pn}, \\ \mathbf{A}_{(2)} &= [(\mathbf{A}^{[1]})^\top, (\mathbf{A}^{[2]})^\top, \dots, (\mathbf{A}^{[n]})^\top] \in \mathbb{R}^{p \times mn}, \\ \mathbf{A}_{(3)} &= [\text{squeeze}(\vec{\mathcal{A}}_1^\top), \dots, \text{squeeze}(\vec{\mathcal{A}}_p^\top)] \in \mathbb{R}^{n \times mp}. \end{aligned}$$

The *multirank* of \mathcal{A} is (r_1, r_2, r_3) with $r_i = \text{rank}(\mathbf{A}_{(i)})$. *Mode- i multiplication* is defined by $\mathcal{C} = \mathcal{A} \times_i \mathbf{B} \Leftrightarrow \mathbf{C}_{(i)} = \mathbf{B}\mathbf{A}_{(i)}$.



Fig. 2.2: **Left:** The $\text{twist}(\cdot)$ operator orients a frontal slice as a lateral slice. **Right:** The $\text{squeeze}(\cdot)$ operator orients a lateral slice as a frontal slice.

2.3. The Tucker Decomposition and HOSVD. The Tucker decomposition of $\mathcal{A} \in \mathbb{R}^{m \times p \times n}$ is defined by

$$\mathcal{A} = \mathcal{G} \times_1 \mathbf{U} \times_2 \mathbf{V} \times_3 \mathbf{W},$$

where $\mathbf{U} \in \mathbb{R}^{m \times r_1}$, $\mathbf{V} \in \mathbb{R}^{p \times r_2}$, $\mathbf{W} \in \mathbb{R}^{n \times r_3}$, and the core tensor $\mathcal{G} \in \mathbb{R}^{r_1 \times r_2 \times r_3}$ [13]. One method for computing this decomposition is the higher-order SVD (HOSVD) [3], outlined in Algorithm 2.1.

Algorithm 2.1 HOSVD [3]

- Compute $\mathbf{A}_{(i)} = \mathbf{Y}_i \boldsymbol{\Sigma}_i \mathbf{Z}_i^\top$ for $i = 1, 2, 3$.
 - Set \mathbf{U} , \mathbf{V} , and \mathbf{W} to be the first r_1 , r_2 , r_3 columns of \mathbf{Y}_1 , \mathbf{Y}_2 , and \mathbf{Y}_3 , respectively, where $r_i = \text{rank}(\mathbf{A}_{(i)})$.
 - Compute $\mathcal{G} = \mathcal{A} \times_1 \mathbf{U}^\top \times_2 \mathbf{V}^\top \times_3 \mathbf{W}^\top$.
-

When the multirank is much smaller than the tensor dimensions, the HOSVD provides an implicitly compressed representation. In this work, we focus on the exact HOSVD and, in particular, on bounds for r_2 , which will be shown to equal the Kronecker rank.

2.4. The Matrix-to-Tensor Framework. We now review the construction of Kilmer and Saibaba [12]. Let $\mathbf{A} \in \mathbb{R}^{(\ell m) \times (qn)}$ be a block-structured matrix with p distinct blocks $\mathbf{A}_k \in \mathbb{R}^{m \times n}$, $k = 1, \dots, p$. Define the *location-tally matrices* $\mathbf{E}_k \in \mathbb{R}^{\ell \times q}$ by

$$(2.2) \quad [\mathbf{E}_k]_{ij} = \begin{cases} 1/\sqrt{\eta_k} & \text{if block } \mathbf{A}_k \text{ occurs at block position } (i, j), \\ 0 & \text{otherwise,} \end{cases}$$

where η_k is the number of occurrences of \mathbf{A}_k . Then,

$$(2.3) \quad \mathbf{A} = \sum_{k=1}^p \mathbf{E}_k \otimes \sqrt{\eta_k} \mathbf{A}_k.$$

A visual representation of Equation (2.3) is given in Figure 2.3 for a block-symmetric block-Toeplitz matrix \mathbf{A} with three distinct blocks.

The *matrix-to-tensor map* $\mathcal{T}: \mathbb{R}^{(\ell m) \times (qn)} \rightarrow \mathbb{R}^{m \times p \times n}$ is defined by setting the k th lateral slice of $\mathcal{A} := \mathcal{T}[\mathbf{A}]$ to

$$(2.4) \quad \vec{\mathcal{A}}_k = \text{twist}(\sqrt{\eta_k} \mathbf{A}_k), \quad k = 1, \dots, p.$$

$$\begin{aligned}
\begin{bmatrix} \mathbf{A}_1 & \mathbf{A}_2 & \mathbf{A}_3 \\ \mathbf{A}_2 & \mathbf{A}_1 & \mathbf{A}_2 \\ \mathbf{A}_3 & \mathbf{A}_2 & \mathbf{A}_1 \end{bmatrix} &= \begin{bmatrix} \mathbf{A}_1 & & \\ & \mathbf{A}_1 & \\ & & \mathbf{A}_1 \end{bmatrix} + \begin{bmatrix} & \mathbf{A}_2 & \\ \mathbf{A}_2 & & \mathbf{A}_2 \\ & \mathbf{A}_2 & \end{bmatrix} + \begin{bmatrix} & & \mathbf{A}_3 \\ & & \\ \mathbf{A}_3 & & \end{bmatrix} \\
&= \underbrace{\left[\frac{1}{\sqrt{3}} \begin{pmatrix} 1 & 0 & 0 \\ 0 & 1 & 0 \\ 0 & 0 & 1 \end{pmatrix} \otimes \sqrt{3} \right]}_{\mathbf{E}_1} \begin{bmatrix} \mathbf{A}_1 & & \\ & \mathbf{A}_1 & \\ & & \mathbf{A}_1 \end{bmatrix} + \underbrace{\left[\frac{1}{\sqrt{4}} \begin{pmatrix} 0 & 1 & 0 \\ 1 & 0 & 1 \\ 0 & 1 & 0 \end{pmatrix} \otimes \sqrt{4} \right]}_{\mathbf{E}_2} \begin{bmatrix} & \mathbf{A}_2 & \\ \mathbf{A}_2 & & \mathbf{A}_2 \\ & \mathbf{A}_2 & \end{bmatrix} + \underbrace{\left[\frac{1}{\sqrt{2}} \begin{pmatrix} 0 & 0 & 1 \\ 0 & 0 & 0 \\ 1 & 0 & 0 \end{pmatrix} \otimes \sqrt{2} \right]}_{\mathbf{E}_3} \begin{bmatrix} & & \mathbf{A}_3 \\ & & \\ \mathbf{A}_3 & & \end{bmatrix}
\end{aligned}$$

$$\mathbf{C}_j = \begin{bmatrix} v_{1,j} & & \\ & v_{2,j} & \\ & & v_{3,j} \end{bmatrix} \begin{bmatrix} \frac{1}{\sqrt{3}} \begin{pmatrix} 1 & 0 & 0 \\ 0 & 1 & 0 \\ 0 & 0 & 1 \end{pmatrix} + \frac{1}{\sqrt{4}} \begin{pmatrix} 0 & 1 & 0 \\ 1 & 0 & 1 \\ 0 & 1 & 0 \end{pmatrix} + \frac{1}{\sqrt{2}} \begin{pmatrix} 0 & 0 & 1 \\ 0 & 0 & 0 \\ 1 & 0 & 0 \end{pmatrix} \end{bmatrix} = \begin{bmatrix} \tilde{v}_{1,j} & \tilde{v}_{3,j} & \tilde{v}_{2,j} \\ \tilde{v}_{2,j} & \tilde{v}_{1,j} & \tilde{v}_{3,j} \\ \tilde{v}_{3,j} & \tilde{v}_{2,j} & \tilde{v}_{1,j} \end{bmatrix}$$

Fig. 2.3: **Top:** Visual representation of Equation (2.3). On the left is a block-symmetric block-Toeplitz matrix \mathbf{A} with three distinct blocks. On the right, \mathbf{A} is written as a sum of Kronecker products of its blocks and the matrices \mathbf{E}_k , as defined in Equation (2.2). **Bottom:** Visual representation of a matrix \mathbf{C}_j described in Theorem 4.1 for the same structure. The elements of \mathbf{C}_j are arranged in the same block pattern as \mathbf{A} . In the right-most matrix, the scaled coefficient $\tilde{v}_{kj} := v_{kj}/\sqrt{\eta_k}$ arises from substituting the definition of \mathbf{E}_k into Equation (2.5).

The inverse *tensor-to-matrix* map $\mathcal{M}: \mathbb{R}^{m \times p \times n} \rightarrow \mathbb{R}^{(\ell m) \times (qn)}$ is

$$\mathcal{M}[\mathcal{A}] = \sum_{k=1}^p \mathbf{E}_k \otimes \text{squeeze}(\vec{\mathcal{A}}_k).$$

If \mathcal{A} admits the Tucker decomposition $\mathcal{A} = \mathcal{G} \times_1 \mathbf{U} \times_2 \mathbf{V} \times_3 \mathbf{W}$ with $\mathcal{G} \in \mathbb{R}^{r_1 \times r_2 \times r_3}$, then

$$(2.5) \quad \mathbf{A} = \mathcal{M}[\mathcal{A}] = \sum_{j=1}^{r_2} \mathbf{C}_j \otimes \mathbf{D}_j,$$

where $\mathbf{C}_j = \sum_{k=1}^p v_{kj} \mathbf{E}_k$, $\mathbf{D}_j = \mathbf{U} \mathbf{G}_j \mathbf{W}^\top$, $v_{kj} = [\mathbf{V}]_{kj}$, and $\mathbf{G}_j = \text{squeeze}(\vec{\mathcal{G}}_j)$. The integer r_2 is thus the number of terms in the Kronecker sum produced by this framework. Figure 2.4 illustrates the full pipeline.

3. Sets, Subspaces, and the Permuted Matrix.

3.1. The Permuted Matrix. By property 4 of the Kronecker product, there exist permutation matrices $\mathbf{P} \in \mathbb{R}^{(\ell m) \times (\ell m)}$ and $\mathbf{Q} \in \mathbb{R}^{(qn) \times (qn)}$ with $\mathbf{P} = \mathbf{S}_{\ell, m}$ and $\mathbf{Q} = \mathbf{S}_{q, n}$ such that

$$\mathbf{P}(\mathbf{E}_k \otimes \sqrt{\eta_k} \mathbf{A}_k) \mathbf{Q}^\top = \sqrt{\eta_k} \mathbf{A}_k \otimes \mathbf{E}_k.$$

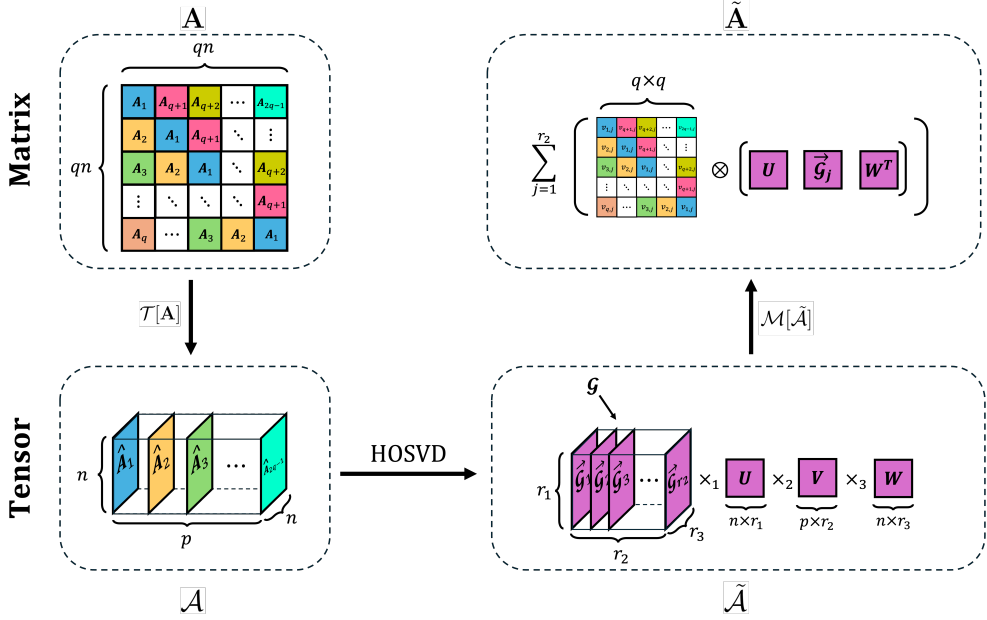


Fig. 2.4: Pipeline for rewriting \mathbf{A} as a sum of Kronecker products via the MTT map, HOSVD, and TTT map of [12].

Define $\mathbf{B} = \mathbf{P}\mathbf{A}\mathbf{Q}^\top \in \mathbb{R}^{(m\ell) \times (nq)}$. This matrix is block-structured with an $m \times n$ grid of blocks each of size $\ell \times q$, and satisfies

$$(3.1) \quad \mathbf{A} = \mathbf{P}^\top \mathbf{B} \mathbf{Q} = \sum_{\kappa=1}^{\rho} \sqrt{\xi_{\kappa}} \mathbf{B}_{\kappa} \otimes \mathbf{F}_{\kappa},$$

where $\mathbf{B}_{\kappa} \in \mathbb{R}^{\ell \times q}$ are the ρ distinct blocks of \mathbf{B} , ξ_{κ} is the multiplicity of \mathbf{B}_{κ} , and $\mathbf{F}_{\kappa} \in \mathbb{R}^{m \times n}$ is the corresponding location-tally matrix. We use k, p for counts associated with \mathbf{A} and κ, ρ for those associated with \mathbf{B} .

Example 3.1. Consider Figure 3.1. On the left, it shows a block-Hankel matrix \mathbf{A} . The matrix has three block-rows and three block-columns, thus $\ell = q = 3$. Each block of \mathbf{A} is a 2×2 Toeplitz matrix, thus $m = n = 2$. By applying appropriate permutation matrices \mathbf{P} and \mathbf{Q}^\top to \mathbf{A} , we get the matrix \mathbf{B} shown on the right. This matrix is a block-Toeplitz matrix with two block-rows and two block-columns, where each block is a 3×3 Hankel matrix. Thus, the permutation matrices have swapped the outer and inner structures of \mathbf{A} .

Let $(\alpha, \beta) \in [m] \times [n]$ and $(\gamma, \delta) \in [\ell] \times [q]$. Let $\mathbf{A}^{(\gamma, \delta)}$ denote the block of \mathbf{A} in block-location (γ, δ) , and $\mathbf{B}^{(\alpha, \beta)}$ the block of \mathbf{B} in block-location (α, β) . The following lemma makes the element-wise relationship between \mathbf{A} and \mathbf{B} precise.

LEMMA 3.2. *Let $\mathbf{A} \in \mathbb{R}^{(\ell m) \times (q n)}$ have lq blocks of size $m \times n$, and let $\mathbf{B} = \mathbf{P}\mathbf{A}\mathbf{Q}^\top$ as above. Then,*

$$(3.2) \quad \mathbf{B}_{\gamma\delta}^{(\alpha, \beta)} = \mathbf{A}_{\alpha\beta}^{(\gamma, \delta)} \quad \text{for all } (\alpha, \beta) \in [m] \times [n], (\gamma, \delta) \in [\ell] \times [q].$$

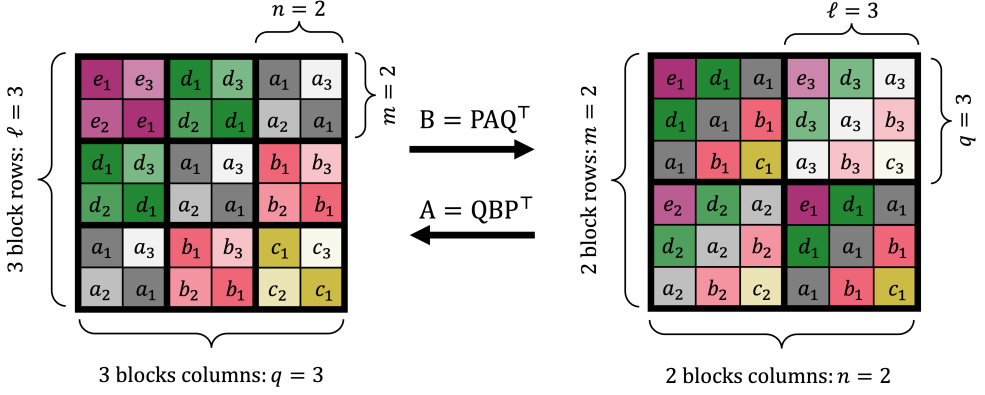


Fig. 3.1: On the left is a block-Hankel matrix \mathbf{A} with Toeplitz blocks. After permuting \mathbf{A} with \mathbf{P} and \mathbf{Q} , we obtain a matrix \mathbf{B} that is block-Toeplitz with Hankel blocks.

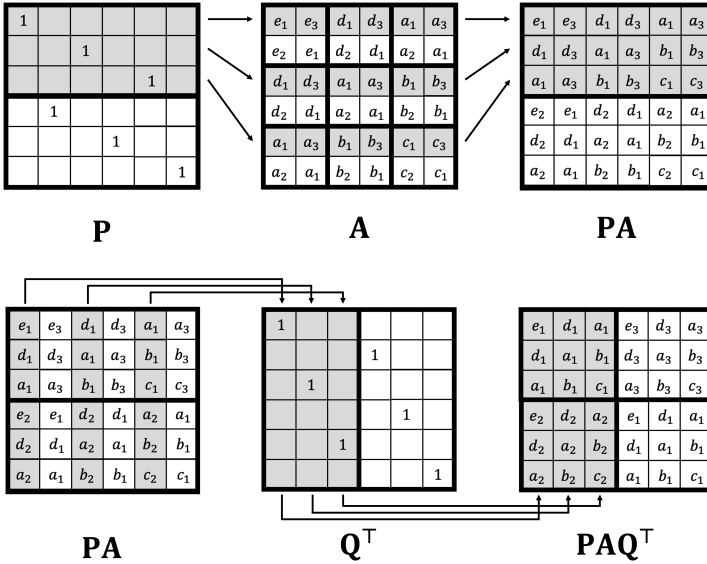


Fig. 3.2: The effects of the permutation matrix \mathbf{P} on the rows of \mathbf{A} (Figure 3.1). The α th block-row of $\mathbf{P} = \mathbf{S}_{\ell, m}$ selects row α from each block-row of \mathbf{A} and consolidates those rows into block-row α of \mathbf{PA} . The matrix \mathbf{Q}^T acts analogously on columns.

Proof. The global row and column indices satisfy

$$(3.3) \quad \mathbf{A}_{\alpha\beta}^{(\gamma, \delta)} = \mathbf{A}_{(\gamma-1)m+\alpha, (\delta-1)n+\beta}, \quad \mathbf{B}_{\gamma\delta}^{(\alpha, \beta)} = \mathbf{B}_{(\alpha-1)\ell+\gamma, (\beta-1)q+\delta}.$$

It therefore suffices to show that

$$(3.4) \quad [\mathbf{PAQ}^T]_{(\alpha-1)\ell+\gamma, (\beta-1)q+\delta} = \mathbf{A}_{(\gamma-1)m+\alpha, (\delta-1)n+\beta}.$$

Action of \mathbf{P} on rows. The shuffle matrix $\mathbf{P} = \mathbf{S}_{\ell, m} \in \mathbb{R}^{(\ell m) \times (\ell m)}$ has block structure: its α th block-row (for $\alpha \in [m]$) consists of ℓ rows, and its γ th row within that block

is the standard basis vector $\mathbf{e}_{(\gamma-1)m+\alpha}^\top$ of length ℓm . Consequently, row $(\alpha-1)\ell + \gamma$ of \mathbf{PA} is row $(\gamma-1)m + \alpha$ of \mathbf{A} :

$$(3.5) \quad [\mathbf{PA}]_{(\alpha-1)\ell+\gamma, j} = \mathbf{A}_{(\gamma-1)m+\alpha, j} \quad \text{for all } j.$$

Action of \mathbf{Q}^\top on columns. By the same reasoning applied to columns, $\mathbf{Q} = \mathbf{S}_{q,n} \in \mathbb{R}^{(qm) \times (qm)}$ satisfies

$$(3.6) \quad [\mathbf{PAQ}^\top]_{i, (\beta-1)q+\delta} = [\mathbf{PA}]_{i, (\delta-1)n+\beta} \quad \text{for all } i.$$

Combining (3.5) and (3.6) with $i = (\alpha-1)\ell + \gamma$ gives (3.4), which is equivalent to (3.2). \square

In the example of Figure 3.1, one may verify directly that $\mathbf{A}_{2,2}^{(2,1)} = \mathbf{B}_{2,1}^{(2,2)} = d_1$, consistent with (3.2).

3.2. Sets and Subspaces. Let $A = \{\mathbf{A}_k\}_{k=1}^p$ be the set of distinct blocks of \mathbf{A} , let $E = \{\mathbf{E}_k\}_{k=1}^p$ be the associated location-tally matrices, let $B = \{\mathbf{B}_\kappa\}_{\kappa=1}^\rho$ be the distinct blocks of \mathbf{B} , and let $F = \{\mathbf{F}_\kappa\}_{\kappa=1}^\rho$ be the corresponding tally matrices.

DEFINITION 3.3. *Define the following four subspaces:*

- $\mathcal{A} = \text{span}(A)$: the inner blockspan of \mathbf{A} ;
- $\mathcal{B} = \text{span}(B)$: the outer blockspan of \mathbf{A} ;
- $\mathcal{E} = \text{span}(E)$: the outer structure space of \mathbf{A} ;
- $\mathcal{F} = \text{span}(F)$: the inner structure space of \mathbf{A} .

PROPOSITION 3.4. *With the notation above, $\mathcal{B} \subseteq \mathcal{E}$ and $\mathcal{A} \subseteq \mathcal{F}$.*

Proof. By Lemma 3.2, each $\mathbf{B}_\kappa \in B$ has entries $b_\kappa^k := [\mathbf{B}_\kappa]_{\gamma\delta}$ (for any (γ, δ) such that $\mathbf{A}^{(\gamma,\delta)} = \mathbf{A}_k$) placed in the same pattern as \mathbf{A}_k occurs in \mathbf{A} . Hence $\mathbf{B}_\kappa = \sum_{k=1}^p b_\kappa^k (\sqrt{\eta_k} \mathbf{E}_k)$, so every generator of \mathcal{B} lies in \mathcal{E} , giving $\mathcal{B} \subseteq \mathcal{E}$. The containment $\mathcal{A} \subseteq \mathcal{F}$ follows by the same argument applied to \mathbf{B} . \square

4. Blockspans and Kronecker Rank. In this section, we state and prove our main theoretical results connecting the blockspans and Kronecker rank.

4.1. Kronecker Rank Equals Dimension of the Inner Blockspan.

THEOREM 4.1. *Let \mathbf{A} be a block-structured matrix with $\ell \times q$ blocks of size $m \times n$, and let $\mathcal{A} = \mathcal{T}[\mathbf{A}]$ be the associated rank- (r_1, r_2, r_3) tensor. Then, $r_2 = \dim(\mathcal{A})$.*

Proof. Since $\vec{\mathcal{A}}_k = \text{twist}(\sqrt{\eta_k} \mathbf{A}_k)$, the i th column of $\sqrt{\eta_k} \mathbf{A}_k$ is the k th column of $\mathbf{A}^{[i]}$, hence the k th row of $(\vec{\mathcal{A}}_k)^\top$. Thus,

$$(4.1) \quad \mathbf{A}_{(2)} = \begin{bmatrix} \mathbf{a}_1^\top \\ \mathbf{a}_2^\top \\ \vdots \\ \mathbf{a}_p^\top \end{bmatrix} \in \mathbb{R}^{p \times mn},$$

where $\mathbf{a}_k = \text{vec}(\sqrt{\eta_k} \mathbf{A}_k)$. See Figure 4.1 for a visualization. Therefore,

$$r_2 = \text{rank}(\mathbf{A}_{(2)}) = \dim(\text{span}\{\mathbf{a}_k\}) = \dim(\text{span}\{\mathbf{A}_k\}) = \dim(\mathcal{A}).$$

This concludes the proof. \square

Remark 4.2. The matrix $\mathbf{A}_{(2)}$ in (4.1) is the reshuffled matrix $\mathcal{R}(\mathbf{A})$ of Van Loan and Pitsianis [14, 15] with (i) rows weighted by $\sqrt{\eta_k}$ and (ii) duplicate rows removed. Both matrices, therefore, have the same row space and the same rank. This is consistent with the equivalence between the two frameworks established in prior work [4, 12].

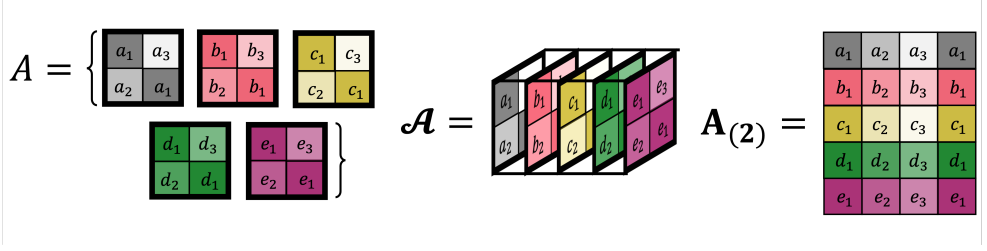


Fig. 4.1: **Left:** The unique blocks of the matrix \mathbf{A} shown in Figure 3.1. **Center:** The tensor \mathcal{A} mapped from \mathbf{A} . **Right:** The second mode unfolding $\mathbf{A}_{(2)}$ of \mathcal{A} .

4.2. Equality of Inner and Outer Blockspan Dimensions: First Proof.

Because $\mathbf{A} = \mathbf{P}^\top \mathbf{B} \mathbf{Q}$, we can write \mathbf{A} as a sum of r_2 or $\bar{r}_2 := \dim(\mathcal{B})$ Kronecker products. The following theorem shows that these two quantities coincide.

THEOREM 4.3. *Let \mathbf{A} be a block-structured matrix and let $\mathbf{B} = \mathbf{P} \mathbf{A} \mathbf{Q}^\top$ as above. Then, $\dim(\mathcal{A}) = \dim(\mathcal{B})$.*

Proof. Let $\bar{r}_2 = \dim(\mathcal{B})$ and let $\{\mathbf{T}_1, \dots, \mathbf{T}_{\bar{r}_2}\}$ be a basis for \mathcal{B} . For each $\mathbf{B}_\kappa \in \mathcal{B}$, write $\mathbf{B}_\kappa = \sum_{j=1}^{\bar{r}_2} \phi_j^\kappa \mathbf{T}_j$. Substituting into (3.1),

$$\mathbf{A} = \sum_{\kappa=1}^{\rho} \sqrt{\xi_\kappa} \left(\sum_{j=1}^{\bar{r}_2} \phi_j^\kappa \mathbf{T}_j \right) \otimes \mathbf{F}_\kappa = \sum_{j=1}^{\bar{r}_2} \mathbf{T}_j \otimes \hat{\mathbf{F}}_j,$$

where $\hat{\mathbf{F}}_j = \sum_{\kappa=1}^{\rho} \phi_j^\kappa \sqrt{\xi_\kappa} \mathbf{F}_\kappa$. Every block $\mathbf{A}^{(\gamma, \delta)} = \sum_{j=1}^{\bar{r}_2} [\mathbf{T}_j]_{\gamma \delta} \hat{\mathbf{F}}_j$ lies in $\text{span}\{\hat{\mathbf{F}}_j\}_{j=1}^{\bar{r}_2}$, so $\dim(\mathcal{A}) \leq \bar{r}_2 = \dim(\mathcal{B})$.

For the reverse inequality, observe that \mathbf{B} is itself a block-structured matrix: it has an $m \times n$ block grid with blocks of size $\ell \times q$. By Lemma 3.2, the (γ, δ) entry of block $\mathbf{B}^{(\alpha, \beta)}$ equals $[\mathbf{A}^{(\gamma, \delta)}]_{\alpha \beta}$; that is, each block of \mathbf{B} is determined by a fixed entry position (α, β) within the blocks of \mathbf{A} . Two positions (α, β) and (α', β') produce the same block of \mathbf{B} if and only if the corresponding entries agree across all blocks of \mathbf{A} , i.e., $[\mathbf{A}^{(\gamma, \delta)}]_{\alpha \beta} = [\mathbf{A}^{(\gamma, \delta)}]_{\alpha' \beta'}$ for all (γ, δ) . The inner blockspan of \mathbf{B} is \mathcal{B} , and its outer blockspan is \mathcal{A} . Applying the preceding argument to \mathbf{B} in place of \mathbf{A} gives $\dim(\mathcal{B}) \leq \dim(\mathcal{A})$, completing the proof. \square

4.3. Equality of Inner and Outer Blockspan Dimensions: Second Proof via Isomorphism. The first proof establishes the equality by a dimension argument. Here we give a second proof by showing that the outer blockspan \mathcal{B} is isomorphic to the column space of $\mathbf{A}_{(2)}$, whose dimension is $r_2 = \dim(\mathcal{A})$ by Theorem 4.1.

Recall from the proof of Proposition 3.4 that each $\mathbf{B}_\kappa \in \mathcal{B}$ satisfies $\mathbf{B}_\kappa = \sum_{k=1}^p b_\kappa^k (\sqrt{\eta_k} \mathbf{E}_k)$. Define two linear maps:

$$(4.2) \quad \text{vec}_{\mathcal{E}}(\mathbf{B}_\kappa) = \begin{bmatrix} \sqrt{\eta_1} b_\kappa^1 \\ \vdots \\ \sqrt{\eta_p} b_\kappa^p \end{bmatrix} \in \mathbb{R}^p \quad \text{and} \quad \text{mat}_{\mathcal{E}}(\mathbf{v}) = \sum_{k=1}^p v_k \mathbf{E}_k, \quad \mathbf{v} \in \mathbb{R}^p.$$

Both maps extend linearly to their respective domains.

LEMMA 4.4. *$\text{vec}_{\mathcal{E}}(\cdot)$ is a linear bijection from \mathcal{B} to $\text{colspace}(\mathbf{A}_{(2)})$, with inverse $\text{mat}_{\mathcal{E}}(\cdot)$. Hence $\mathcal{B} \cong \text{colspace}(\mathbf{A}_{(2)})$.*

Proof. Step 1: $\text{vec}_\mathcal{E}$ maps \mathcal{B} into $\text{colspace}(\mathbf{A}_{(2)})$. Every $\mathbf{T} \in \mathcal{B}$ writes as $\mathbf{T} = \sum_{\kappa} \zeta_{\kappa} \mathbf{B}_{\kappa}$, so by linearity

$$\text{vec}_\mathcal{E}(\mathbf{T}) = \sum_{\kappa=1}^{\rho} \zeta_{\kappa} \begin{bmatrix} \sqrt{\eta_1} b_{\kappa}^1 \\ \vdots \\ \sqrt{\eta_p} b_{\kappa}^p \end{bmatrix}.$$

By Equation (4.1), column (α, β) of $\mathbf{A}_{(2)}$ is the vector $([\mathbf{A}_1]_{\alpha\beta\sqrt{\eta_1}}, \dots, [\mathbf{A}_p]_{\alpha\beta\sqrt{\eta_p}})^{\top}$. By Lemma 3.2, $[\mathbf{B}_{\kappa}]_{\gamma\delta} = [\mathbf{A}^{(\gamma,\delta)}]_{\alpha\beta}$ for any (α, β) with $\mathbf{B}^{(\alpha,\beta)} = \mathbf{B}_{\kappa}$, so $(\sqrt{\eta_1} b_{\kappa}^1, \dots, \sqrt{\eta_p} b_{\kappa}^p)^{\top}$ is exactly column (α, β) of $\mathbf{A}_{(2)}$. Two distinct blocks $\mathbf{B}_{\kappa} \neq \mathbf{B}_{\kappa'}$ produce distinct column vectors (if they agreed entrywise, they would not be distinct blocks by definition); multiple positions (α, β) with the same block \mathbf{B}_{κ} produce identical columns, but the span is unchanged. Hence $\text{vec}_\mathcal{E}(\mathbf{T}) \in \text{colspace}(\mathbf{A}_{(2)})$ and thus $\text{vec}_\mathcal{E}(\mathcal{B}) \subseteq \text{colspace}(\mathbf{A}_{(2)})$.

Step 2: $\text{mat}_\mathcal{E}$ maps $\text{colspace}(\mathbf{A}_{(2)})$ into \mathcal{B} . By Equation (4.1), column (i, j) of $\mathbf{A}_{(2)}$ is $\mathbf{c}_{ij} = ([\mathbf{A}_1]_{ij\sqrt{\eta_1}}, \dots, [\mathbf{A}_p]_{ij\sqrt{\eta_p}})^{\top}$. Applying $\text{mat}_\mathcal{E}$ gives

$$\text{mat}_\mathcal{E}(\mathbf{c}_{ij}) = \sum_{k=1}^p [\mathbf{A}_k]_{ij\sqrt{\eta_k}} \mathbf{E}_k.$$

By Lemma 3.2, the (γ, δ) entry of the block $\mathbf{B}^{(i,j)}$ of \mathbf{B} equals $[\mathbf{A}^{(\gamma,\delta)}]_{ij}$. Summing over k with the location-tally weights shows that $\text{mat}_\mathcal{E}(\mathbf{c}_{ij})$ is precisely the matrix $\mathbf{B}^{(i,j)}$, which belongs to $B \subset \mathcal{B}$. Since $\text{colspace}(\mathbf{A}_{(2)})$ is spanned by $\{\mathbf{c}_{ij}\}$, linearity gives $\text{mat}_\mathcal{E}(\text{colspace}(\mathbf{A}_{(2)})) \subseteq \mathcal{B}$.

Step 3: The maps are mutual inverses. A direct substitution verifies

$$\text{mat}_\mathcal{E}(\text{vec}_\mathcal{E}(\mathbf{B}_{\kappa})) = \mathbf{B}_{\kappa} \text{ and } \text{vec}_\mathcal{E}(\text{mat}_\mathcal{E}(\mathbf{v})) = \mathbf{v},$$

so they are inverse bijections, establishing $\mathcal{B} \cong \text{colspace}(\mathbf{A}_{(2)})$. \square

Theorem 4.3 follows immediately: $\dim(\mathcal{B}) = \dim(\text{colspace}(\mathbf{A}_{(2)})) = r_2 = \dim(\mathcal{A})$.

5. Structure-Informed and Sparsity-Informed Bounds.

5.1. Structural Bounds. From Theorem 4.1, the Kronecker rank $r_2 = \dim(\mathcal{A})$. When the blocks of \mathbf{A} are not known explicitly, one can bound $\dim(\mathcal{A})$ by working with larger spaces defined by the structural type of the blocks.

Let \mathcal{S} denote the subspace of matrices whose form is determined by the structural type of the blocks of \mathbf{A} (e.g., the space of $m \times n$ Toeplitz matrices if each block is Toeplitz), and let \mathcal{T} denote the analogous space for the outer block structure (i.e., the structural type of the blocks of \mathbf{B}). By construction, $\mathcal{A} \subseteq \mathcal{S} \subseteq \mathcal{F}$ and $\mathcal{B} \subseteq \mathcal{T} \subseteq \mathcal{E}$.

COROLLARY 5.1. *With \mathcal{S} and \mathcal{T} defined as above,*

$$r_2 \leq \min\{\dim(\mathcal{S}), \dim(\mathcal{T})\}.$$

Figure 5.1 illustrates these containments.

Remark 5.2. The distinction between \mathcal{T} and \mathcal{E} is important. The set \mathcal{E} is built from the *distinct* blocks of \mathbf{A} in the elementwise sense, whereas \mathcal{T} is defined by linear structure. For example, if \mathbf{A} has a symmetric block-Toeplitz-plus-Hankel outer structure then \mathcal{T} is the space of $q \times q$ symmetric Toeplitz-plus-Hankel matrices with $\dim(\mathcal{T}) = 2q - 2$, while \mathbf{A} has $(q^2/4) + (q/2)$ distinct blocks giving $\dim(\mathcal{E}) = (q^2/4) + (q/2)$ (see Appendix A for the derivation of this formula in the case $q = 5$). For $q \geq 5$ we have $\mathcal{T} \subsetneq \mathcal{E}$, and $\dim(\mathcal{T})$ gives a strictly tighter bound.

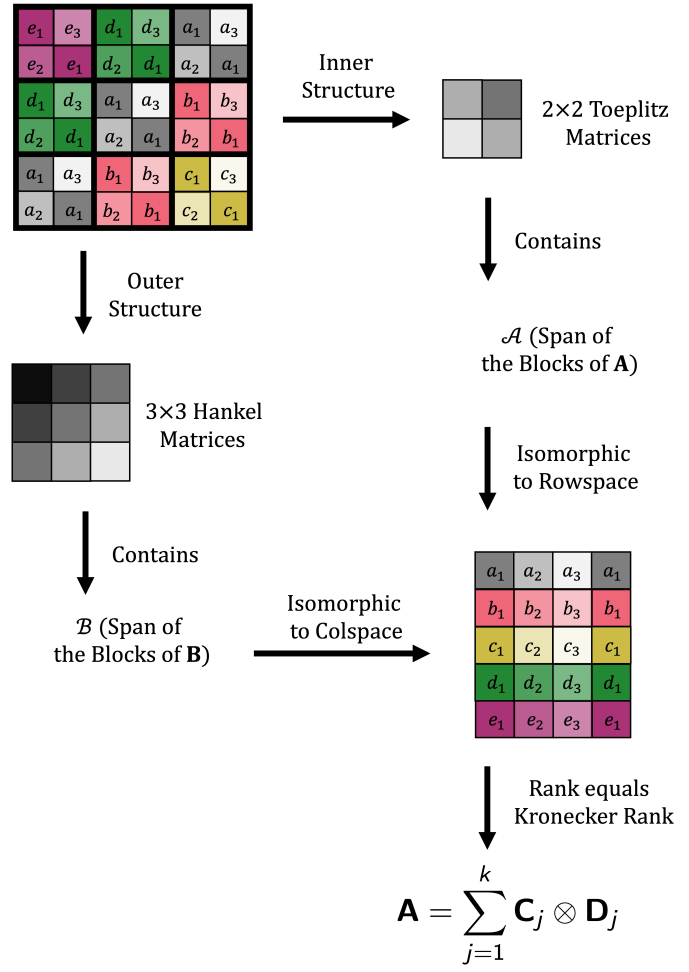


Fig. 5.1: The nested containments $\mathcal{A} \subseteq \mathcal{S} \subseteq \mathcal{F}$ and $\mathcal{B} \subseteq \mathcal{T} \subseteq \mathcal{E}$ connecting structural spaces to the Kronecker rank. Dimensions of \mathcal{S} and \mathcal{T} provide computable upper bounds on r_2 .

Remark 5.3. Similarly, $\dim(\mathcal{A}) \leq \dim(\mathcal{S})$ and the inequality can be strict. For instance, if all blocks of \mathbf{A} are scalar multiples of a single matrix, then $\dim(\mathcal{A}) = 1$ regardless of what structural type the blocks possess.

Table of bounds. Table 5.1 records $\dim(\mathcal{T})$ and $\dim(\mathcal{S})$ for three representative matrix families, for two choices of q (outer block grid size) and n (block size). The tighter of the two bounds is highlighted. All formulas assume that q and n are even.

5.2. Sparsity-Informed Bounds. When the blocks of \mathbf{A} are sparse, the rank of $\mathbf{A}_{(2)}$ is bounded by the number of positions that are nonzero in *at least one* block. This is formalized in the following theorem.

THEOREM 5.4. *Let $\mathbf{A} \in \mathbb{R}^{(\ell m) \times (qn)}$ be a block-structured matrix. For each distinct*

	Inner struct.	Outer struct.	dim(\mathcal{T})	dim(\mathcal{S})	min
$\mathbf{q} = \mathbf{32}$ $\mathbf{n} = \mathbf{64}$	Sym. T+H	Nonsym. T+H	62	252	62
	Nonsym. T+H	Sym. Toeplitz	124	64	64
	Nonsym. T+H	Tridiagonal	124	190	124
$\mathbf{q} = \mathbf{64}$ $\mathbf{n} = \mathbf{32}$	Sym. T+H	Nonsym. T+H	126	124	124
	Nonsym. T+H	Sym. Toeplitz	252	32	32
	Nonsym. T+H	Tridiagonal	252	94	94

Table 5.1: Structural upper bounds on r_2 for three matrix families and two block-size combinations. “Sym. T+H” = symmetric Toeplitz plus persymmetric Hankel; “Nonsym. T+H” = Toeplitz-plus-Hankel without symmetry conditions. The overall bound is $\min\{\dim(\mathcal{T}), \dim(\mathcal{S})\}$.

block \mathbf{A}_k , define the nonzero index set $C_k := \{(i, j) \mid [\mathbf{A}_k]_{ij} \neq 0\}$. Then,

$$r_2 \leq \text{card}\left(\bigcup_{k=1}^p C_k\right).$$

Proof. Let $c = \text{card}(\bigcup_k C_k)$. By Equation (4.1), each row of $\mathbf{A}_{(2)}$ is $\mathbf{a}_k = \text{vec}(\sqrt{\eta_k} \mathbf{A}_k)$. A column of $\mathbf{A}_{(2)}$, indexed by position (i, j) , is zero if $[\mathbf{A}_k]_{ij} = 0$ for all k , i.e., if $(i, j) \notin \bigcup_k C_k$. Hence $\mathbf{A}_{(2)}$ has at most c nonzero columns, giving $r_2 \leq c$. \square

When all blocks share the same sparsity pattern, $\bigcup_k C_k = C_k$ for any k , so $r_2 \leq \text{nnz}(\mathbf{A}_k)$. For banded blocks, the following corollary applies immediately.

COROLLARY 5.5. *Let each block \mathbf{A}_k have upper bandwidth u_k and lower bandwidth ℓ_k , and set $b_u = \max_k u_k$, $b_\ell = \max_k \ell_k$. Then,*

$$r_2 \leq n + \sum_{i=1}^{b_u} (n - i) + \sum_{j=1}^{b_\ell} (n - j).$$

We can also establish a relationship between the sparsity within the blocks of \mathbf{A} and the block-sparsity of the permuted matrix \mathbf{B} . Here, block-sparsity refers to the ratio of nonzero blocks to the total number of blocks. To do so, we present the following theorem.

THEOREM 5.6. *Let \mathbf{A} be a block-structured matrix and let \mathbf{B} be the matrix permuted from \mathbf{A} such that the inner and outer structures have been swapped. Define the sets C_k as above and similarly define the sets D_κ corresponding to the blocks of \mathbf{B} , i.e., $D_\kappa := \{(i, j) \mid [\mathbf{B}_\kappa]_{ij} \neq 0\}$. Finally, let η_k and ξ_κ be the number of times that block \mathbf{A}_k and \mathbf{B}_κ repeat in \mathbf{A} and \mathbf{B} , respectively. Then,*

$$\text{card}\left(\bigcup_{k=1}^p C_k\right) = \sum_{\kappa=1}^p \xi_\kappa, \quad \text{card}\left(\bigcup_{\kappa=1}^p D_\kappa\right) = \sum_{k=1}^p \eta_k.$$

Proof. We prove the first equality; the second follows by applying the same argu-

ment to \mathbf{B} . Define

$$\overline{\bigcup_{k=1}^p C_k} = \{(i, j) \in [m] \times [n] \mid [\mathbf{A}_k]_{ij} = 0 \text{ for all } k\}.$$

For each κ , let $\{(\alpha, \beta)\}_{\kappa} = \{(\alpha, \beta) \mid \mathbf{B}^{(\alpha, \beta)} = \mathbf{B}_{\kappa}\}$, so $\text{card}(\{(\alpha, \beta)\}_{\kappa}) = \xi_{\kappa}$.

Step 1. If $(\alpha, \beta) \in \overline{\bigcup_k C_k}$, then $[\mathbf{B}^{(\alpha, \beta)}]_{\gamma\delta} = [\mathbf{A}^{(\gamma, \delta)}]_{\alpha\beta} = 0$ for all (γ, δ) , so $\mathbf{B}^{(\alpha, \beta)} = \mathbf{0} \notin B$.

Step 2. We claim the sets $\{(\alpha, \beta)\}_{\kappa}$ partition $\bigcup_k C_k$. *Coverage:* if $(\alpha, \beta) \in \bigcup_k C_k$, then some entry of $\mathbf{B}^{(\alpha, \beta)}$ is nonzero (by Lemma 3.2), so $\mathbf{B}^{(\alpha, \beta)} \in B$ and $(\alpha, \beta) \in \{(\alpha, \beta)\}_{\kappa}$ for some κ . For the reverse, let $(\alpha, \beta) \in \{(\alpha, \beta)\}_{\kappa}$ for an arbitrary choice of κ . Suppose that $(\alpha, \beta) \in \overline{\bigcup_k C_k}$. Since $(\alpha, \beta) \in \{(\alpha, \beta)\}_{\kappa}$, there exists some $\kappa \in [\rho]$ such that $\mathbf{B}^{(\alpha, \beta)} = \mathbf{B}_{\kappa}$. However, this contradicts Step 1. Thus, (α, β) must not be in the set $\overline{\bigcup_k C_k}$ and then must be in the set $\bigcup_k C_k$. *Disjointness:* if $(\alpha, \beta) \in \{(\alpha, \beta)\}_{\kappa_1} \cap \{(\alpha, \beta)\}_{\kappa_2}$ then $\mathbf{B}_{\kappa_1} = \mathbf{B}^{(\alpha, \beta)} = \mathbf{B}_{\kappa_2}$, contradicting distinctness for $\kappa_1 \neq \kappa_2$.

$$\text{Hence } \text{card}(\bigcup_k C_k) = \sum_{\kappa} \text{card}(\{(\alpha, \beta)\}_{\kappa}) = \sum_{\kappa} \xi_{\kappa}. \quad \square$$

6. Numerical Examples.

6.1. BTHTHB Matrices: Verifying the Theory. Matrices with Block-Toeplitz-plus-Hankel structure with Toeplitz-plus-Hankel blocks (BTHTHB) arise in image deblurring [7, 11, 18]. We verify Corollary 5.1 by comparing the theoretical bound r_{th} (derived from structure) with the numerically computed rank $r_{calc} = \text{rank}(\mathbf{A}_{(2)})$ for four BTHTHB structures.

Let $\mathbf{A} \in \mathbb{R}^{n^2 \times n^2}$ be BTHTHB with $n \times n$ blocks and *random entries*, so that any dependence among the blocks of \mathbf{A} is attributable to structure alone. Write $\mathbf{A} = \mathbf{A}_T + \mathbf{A}_H$ where \mathbf{A}_T is block-Toeplitz and \mathbf{A}_H is block-Hankel. Letting $\nu \sim \mathcal{N}(0, 1)$ independently, we construct

$$\mathbf{A} = \left(\sum_i \tilde{\mathbf{E}}_{T_i} \otimes \sum_j \nu_j \tilde{\mathbf{E}}_{T_j} \right) + \left(\sum_k \tilde{\mathbf{E}}_{H_k} \otimes \sum_{\ell} \nu_{\ell} \tilde{\mathbf{E}}_{H_{\ell}} \right),$$

where $\tilde{\mathbf{E}}_{(\cdot)}$ are the unscaled location-tally matrices. The four structures tested (illustrated in Figure 6.1) are:

- *Symmetric Full:* \mathbf{A}_T full and block-symmetric and \mathbf{A}_H full and block-persymmetric.
- *Nonsymmetric Full:* same, without symmetry or persymmetry.
- *Symmetric Banded:* \mathbf{A}_T block-banded with upper bandwidth $n/2 - 1$, lower bandwidth $n/2$ (nearly symmetric); \mathbf{A}_H analogously banded (nearly persymmetric).
- *Nonsymmetric Banded:* as above, without the symmetry conditions.

The results are shown in Table 6.1. In the center columns, we compare r_{th} to p and r_{calc} , the rank of $\mathbf{A}_{(2)}$ as calculated by the MATLAB `rank` command. Agreement $r_{th} = r_{calc}$ holds in all cases, confirming that our structural bounds are exact. The relative error between \mathbf{A} and the reconstruction $\tilde{\mathbf{A}}$ using only r_{th} Kronecker terms was on the order of 10^{-15} in all cases.

6.2. Sparsity Bounds. We now illustrate Theorem 5.4 for small examples with $q = 4$ and $n = 8$.

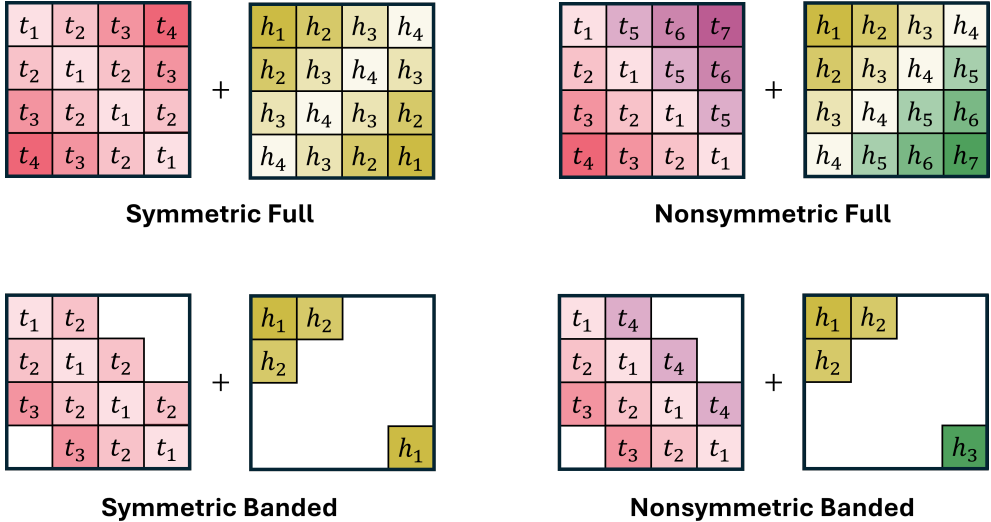


Fig. 6.1: The four BTHTHB structures for $n = 4$.

Shared sparsity pattern. Let $\mathbf{A} \in \mathbb{R}^{n^2 \times n^2}$ be a block-dense matrix whose blocks all share the same sparsity pattern at level $\tau = 0.3$, with entries drawn independently from $\mathcal{N}(0, 1)$. Since the blocks share a single pattern, $\bigcup_k C_k = C_1$ and the sparsity bound gives $c = \lfloor \tau n^2 \rfloor = 19$. Because there is no repeated outer block structure, the outer block space is the full space of $q \times q$ matrices, giving $\dim(\mathcal{B}) = q^2 = 16$ as a crude structural upper bound. Here, the structural bound is tighter: $r_2 \leq \min\{19, 16\} = 16$.

For $\tau = 0.2$ the sparsity bound becomes $c = \lfloor 0.2 \cdot 64 \rfloor = 12$, while the structural bound remains $q^2 = 16$. Now sparsity governs: $r_2 \leq 12$.

Differing sparsity patterns. Finally, suppose each block has a distinct sparsity pattern, but each has exactly 7 nonzero entries. The union $\bigcup_k C_k$ is then precisely the set of positions that are nonzero in at least one block; if the union has the same cardinality as in the $\tau = 0.2$ case above, the bound $r_2 \leq 12$ applies equally.

Figure 6.2 shows spy plots of \mathbf{A} (left column) and $\mathbf{A}_{(2)}$ (right column) for each case, confirming the predicted number of nonzero columns.

6.3. Explaining Singular Value Decay in SuiteSparse Matrices. We now revisit two examples from [12] in which the authors demonstrate compression of sparse matrices from the SuiteSparse collection [2]. While that work attributes the compression to rapid decay of the singular values of $\mathbf{A}_{(2)}$, it does not explain *why* the decay occurs. Our theory provides that explanation.

Matrix t2d_q4. This finite-difference matrix for nonlinear diffusion is sparse and block-tridiagonal. It is block 99×99 , with each block also of size 99×99 . The associated tensor satisfies $\mathcal{A} \in \mathbb{R}^{99 \times 295 \times 99}$; a naive mapping would yield 295 Kronecker terms. Kilmer and Saibaba showed that compressing the second mode to rank 5 caused negligible error.

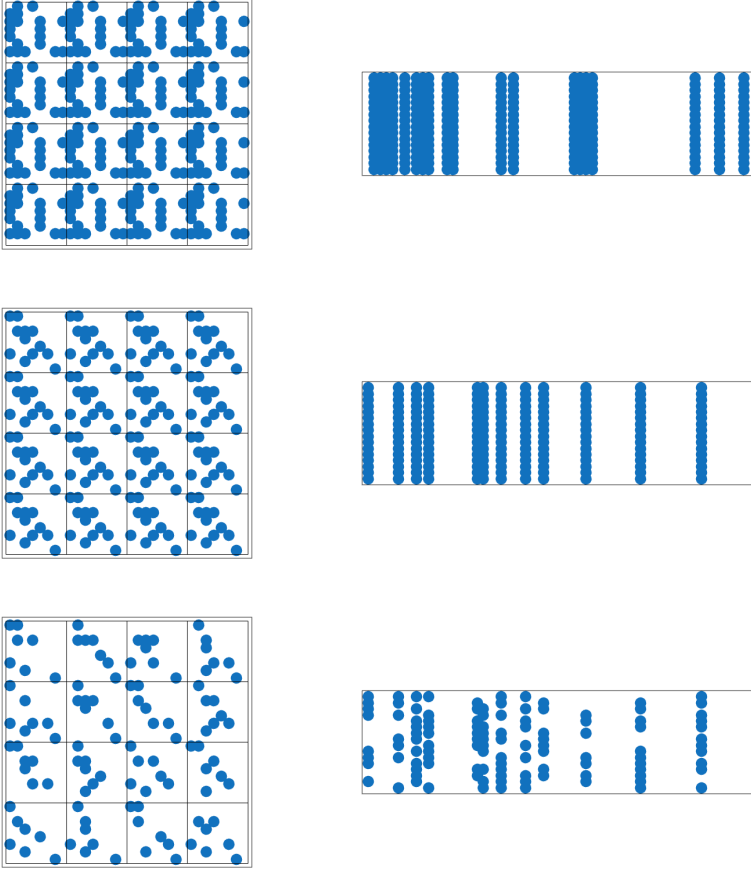


Fig. 6.2: Left column: spy plots of \mathbf{A} . Right column: corresponding spy plots of $\mathbf{A}_{(2)}$, confirming the predicted number of nonzero columns in each case. Top row ($\tau = 0.3$, shared pattern): the structural bound $q^2 = 16$ is tighter than the sparsity bound $c = 19$. Middle row ($\tau = 0.2$, shared pattern): the sparsity bound $c = 12$ governs. Bottom row (differing patterns, union of cardinality 12): the sparsity bound again gives $r_2 \leq 12$.

Every diagonal block satisfies $\mathbf{A}_{d_k} = \Phi_d + x_k \Phi_c$, and every off-diagonal block satisfies $\mathbf{A}_{o_k} = \Phi_o + x_k \Phi_c$. Thus $\{\Phi_d, \Phi_o, \Phi_c\}$ spans all blocks of \mathbf{A} except possibly \mathbf{A}_y . These three matrices are linearly independent: Φ_c is supported only at position $(99, 99)$, while Φ_d and Φ_o are zero there and differ on the interior diagonal entries $(8/3$ vs. $-1/3)$, so no nontrivial linear combination can vanish.

If $\mathbf{A}_y \in \text{span}\{\Phi_d, \Phi_o, \Phi_c\}$, then all blocks lie in a three-dimensional subspace and $r_2 \leq 3$. If $\mathbf{A}_y \notin \text{span}\{\Phi_d, \Phi_o, \Phi_c\}$, it contributes exactly one additional dimension. In either case,

$$\mathcal{A} \subseteq \text{span}\{\Phi_d, \Phi_o, \Phi_c, \mathbf{A}_y\},$$

giving $\dim(\mathcal{A}) \leq 4$, and by Theorem 4.1, $r_2 \leq 4$.

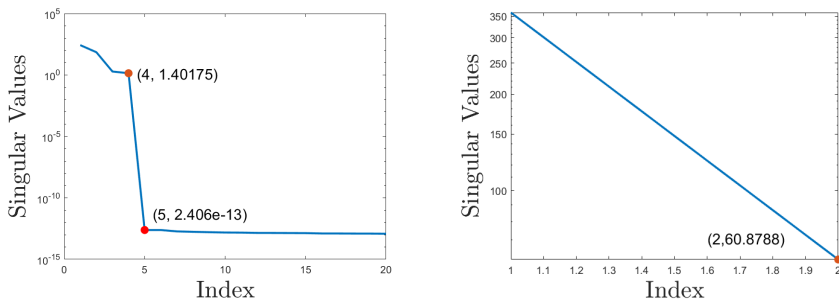


Fig. 6.3: Left: First 20 singular values of $\mathbf{A}_{(2)}$ for `t2d.q4`. Right: Singular values of $\mathbf{A}_{(2)}$ for `fv2`.

Figure 6.3 (left) plots the first 20 singular values of $\mathbf{A}_{(2)}$, confirming that the numerical rank is exactly 4. Our structural analysis thus provides a tight bound and fully explains the rapid singular value decay reported in [12].

Matrix fv2. We now consider the matrix `fv2` from the SuiteSparse collection, which has the form

$$\mathbf{A} = \begin{bmatrix} \mathbf{A}_d & \mathbf{A}_o & & & \\ \mathbf{A}_o & \mathbf{A}_d & \mathbf{A}_o & & \\ & \ddots & \ddots & \ddots & \\ & & \mathbf{A}_o & \mathbf{A}_d & \mathbf{A}_o \\ & & & \mathbf{A}_o & \mathbf{A}_d \end{bmatrix},$$

where the only two distinct blocks \mathbf{A}_d and \mathbf{A}_o are

$$\mathbf{A}_d = \begin{bmatrix} 3.5101 & -0.5 & & & \\ -0.5 & \ddots & \ddots & & \\ & \ddots & \ddots & -0.5 & \\ & & -0.5 & 3.5101 & \end{bmatrix} \quad \text{and} \quad \mathbf{A}_o = \begin{bmatrix} 0.5 & -0.25 & & & \\ -0.25 & \ddots & \ddots & & \\ & \ddots & \ddots & -0.25 & \\ & & -0.25 & 0.5 & \end{bmatrix}.$$

This matrix is block-symmetric and block-tridiagonal, with symmetric tridiagonal blocks whose diagonals are constant. The outer structure is therefore a symmetric Toeplitz tridiagonal pattern of dimension 2, and the inner structure has the same dimension. Hence $r_2 = \dim(\mathcal{A}) = 2$, and \mathbf{A} can be written exactly as a sum of two Kronecker products. Figure 6.3 (right) confirms that $\mathbf{A}_{(2)}$ has exactly two nonzero singular values.

7. Conclusion. We have derived a complete characterization of the Kronecker rank of a block-structured matrix in terms of its underlying structure. The central result is the chain $r_2 = \dim(\mathcal{A}) = \dim(\mathcal{B})$, proved both by a direct dimension argument and via an explicit isomorphism between the outer blockspan and the column space of the second-mode unfolding. The nested containments $\mathcal{A} \subseteq \mathcal{S} \subseteq \mathcal{F}$ and $\mathcal{B} \subseteq \mathcal{T} \subseteq \mathcal{E}$ translate structural and sparsity information into computable upper bounds on r_2 . For two sparse matrices from the SuiteSparse collection, these bounds are tight and provide a structural explanation for singular value decay that had previously been

observed but not understood.

Several directions for future work remain open. First, extending the isomorphism proof to matrices with *multiple levels* of nested block structure would generalize the framework to higher-order Tucker decompositions. Second, the preliminary analysis of modes 1 and 3 of the associated tensor, which can exhibit rank deficiency when the blocks of \mathbf{A} are themselves low-rank, warrants further investigation; a full characterization of this case could enable additional compression beyond the second mode. Third, a systematic study of the conditions under which $\dim(\mathcal{A}) < \dim(\mathcal{S})$ (i.e., when the actual Kronecker rank is strictly below the structural bound) would be practically useful.

Acknowledgments. ME was supported through a Karen EDGE Fellowship. MK acknowledges support from NSF DMS 2410698.

Appendix A. A Worked Example: Toeplitz-plus-Hankel Outer Structure.

We revisit the remark from Section 5.1. We demonstrate why $\mathcal{T} \subsetneq \mathcal{E}$ for a matrix with a block 5×5 symmetric-Toeplitz-plus-persymmetric-Hankel outer structure and show in this case that $\dim(\mathcal{E}) = 9$ while $\dim(\mathcal{T}) = 8$.

Counting distinct blocks and deriving $\dim(\mathcal{E})$. A 5×5 symmetric Toeplitz matrix \mathbf{A}_T satisfies $[\mathbf{A}_T]_{\gamma\delta} = t_{|\gamma-\delta|}$ for parameters t_0, \dots, t_4 , giving 5 free parameters. A 5×5 persymmetric Hankel matrix \mathbf{A}_H satisfies $[\mathbf{A}_H]_{\gamma\delta} = h_{\gamma+\delta-1}$ for parameters h_1, \dots, h_5 , also giving 5 free parameters. In the sum $\mathbf{C} = \mathbf{A}_T + \mathbf{A}_H$, an entry $[\mathbf{C}]_{\gamma\delta}$ depends on the pair $(|\gamma - \delta|, \gamma + \delta - 1)$. Table A.1 lists all distinct such pairs for $\gamma, \delta \in \{1, \dots, 5\}$; direct enumeration yields exactly 9 distinct pairs (the pair $(0, 5)$ at $\gamma = \delta = 3$ is the one whose constraint is derived below), giving $p = 9$ distinct block positions. Since the location-tally matrices $\{\mathbf{E}_k\}_{k=1}^9$ each record a distinct pattern of block positions and are therefore linearly independent, $\dim(\mathcal{E}) = 9$. For general even q , the analogous count gives $\dim(\mathcal{E}) = q^2/4 + q/2$.

Position (γ, δ) (representative)	$ \gamma - \delta $	$\gamma + \delta - 1$
(1, 1)	0	1
(1, 2), (2, 1)	1	2
(1, 3), (3, 1)	2	3
(1, 4), (4, 1)	3	4
(1, 5), (5, 1)	4	5
(2, 2)	0	3
(2, 3), (3, 2)	1	4
(2, 4), (4, 2)	2	5
(3, 3)	0	5

Table A.1: The 9 distinct $(|\gamma - \delta|, \gamma + \delta - 1)$ pairs for a 5×5 symmetric-Toeplitz-plus-persymmetric-Hankel matrix, confirming $\dim(\mathcal{E}) = 9$. The remaining positions, such as $(2, 5), (3, 4), (3, 5), (4, 5)$ and their transposes, produce pairs such as $(3, 6), (1, 6), (2, 7), (3, 8)$ that are already listed above: Toeplitz symmetry identifies $t_{|\gamma-\delta|}$ with the same parameter for transposed positions, and Hankel persymmetry identifies $h_{\gamma+\delta-1}$ for positions with the same antidiagonal sum. These structural identifications reduce the 25 block positions to the 9 listed pairs without introducing new independent parameters.

The linear constraint and $\dim(\mathcal{J})$. Label the nine distinct entry values of a generic $\mathbf{C} = \mathbf{A}_T + \mathbf{A}_H$ as $\gamma_i = t_{i-1} + h_{6-i}$ for $i = 1, \dots, 5$, and $\gamma_6 = t_1 + h_3$, $\gamma_7 = t_2 + h_2$, $\gamma_8 = t_3 + h_1$, $\gamma_9 = t_0 + h_4$. (Here γ_9 is the center entry $[\mathbf{C}]_{3,3} = t_0 + h_4$.) These nine values are not independent: they satisfy the linear relation

$$(A.1) \quad \gamma_6 + \gamma_8 - \gamma_3 = (t_1 + h_3) + (t_3 + h_1) - (t_3 + h_3) = t_1 + h_1 = \gamma_9,$$

so $\dim(\mathcal{J}) = 8$. In contrast, \mathcal{E} imposes no such relation, giving $\dim(\mathcal{E}) = 9 > \dim(\mathcal{J}) = 8$. The matrix \mathbf{X} obtained from \mathbf{C} by replacing the third-column (and third-row) entries with an independent value $t_6 + h_6 \neq t_3 + h_3$ lies in \mathcal{E} but violates (A.1), confirming $\mathcal{J} \subsetneq \mathcal{E}$.

LEMMA A.1. *Let $\mathbf{X} \in \mathcal{E}$ with entries labeled $\gamma_1, \dots, \gamma_9$ as above. Then $\mathbf{X} \in \mathcal{J}$ if and only if $\gamma_9 = \gamma_6 + \gamma_8 - \gamma_3$.*

Proof. Only if. If $\mathbf{X} = \mathbf{T} + \mathbf{H}$ with \mathbf{T} symmetric Toeplitz and \mathbf{H} persymmetric Hankel, then the labeling above gives (A.1) directly.

If. Suppose $\gamma_9 = \gamma_6 + \gamma_8 - \gamma_3$. We construct explicit Toeplitz and Hankel parameters. Set

$$(A.2) \quad t_0 = \gamma_1, \quad t_1 = \gamma_6 - h_3, \quad t_2 = \gamma_7 - h_2, \quad t_3 = \gamma_8 - h_1, \quad t_4 = \gamma_5 - h_1,$$

where the Hankel parameters are determined by

$$(A.3) \quad h_5 = \gamma_1 - t_0, \quad h_4 = \gamma_2 - t_1, \quad h_3 = \gamma_3 - t_2, \quad h_2 = \gamma_4 - t_3, \quad h_1 = \gamma_5 - t_4.$$

We must verify that this system is consistent. From (A.3), $h_3 = \gamma_3 - t_2$ and $h_1 = \gamma_5 - t_4$. Substituting into $t_1 = \gamma_6 - h_3$ gives $t_1 = \gamma_6 - \gamma_3 + t_2$, and substituting into $t_3 = \gamma_8 - h_1$ gives $t_3 = \gamma_8 - \gamma_5 + t_4$. These are two equations in t_0, \dots, t_4 and h_1, \dots, h_5 . The system has a free parameter (say t_0); choosing $t_0 = \gamma_1 - h_5$ with $h_5 = \gamma_1 - t_0$ means h_5 is determined once t_0 is chosen. Setting $h_5 = 0$ fixes $t_0 = \gamma_1$, from which all other parameters follow uniquely. Under the constraint $\gamma_9 = \gamma_6 + \gamma_8 - \gamma_3$, one verifies directly that $[\mathbf{T}]_{33} = t_0$ and $[\mathbf{H}]_{33} = h_4 = \gamma_9 - t_0$, giving $[\mathbf{T} + \mathbf{H}]_{33} = \gamma_9$, as required. All other entries follow from the Toeplitz and Hankel structure by construction. Therefore $\mathbf{X} = \mathbf{T} + \mathbf{H} \in \mathcal{J}$. \square

REFERENCES

- [1] Grey Ballard and Tamara G. Kolda. *Tensor Decompositions for Data Science*. Cambridge University Press, 2025.
- [2] Timothy A. Davis and Yifan Hu. The University of Florida sparse matrix collection. *ACM Trans. Math. Softw.*, 38(1), 2011.
- [3] Lieven De Lathauwer, Bart De Moor, and Joos Vandewalle. A multilinear singular value decomposition. *SIAM Journal on Matrix Analysis and Applications*, 21(4):1253–1278, 2000.
- [4] Allison Fuller. *Tensor-Based Kronecker Rank Analysis of Structured Matrices with Applications to Inverse Problems*. ProQuest Dissertations & Theses, 2026.
- [5] Alexander Graham. *Kronecker Products and Matrix Calculus with Applications*. Dover Books on Mathematics. Dover Publications, 2018.
- [6] Wolfgang Hackbusch, Boris N. Khoromskij, and Eugene E. Tyrtyshnikov. Hierarchical Kronecker tensor-product approximations. *Max Plank Insitutue*, 2003.
- [7] Per Christian Hansen, James G. Nagy, and Dianne P. O’Leary. *Deblurring Images*. Society for Industrial and Applied Mathematics, Philidelphia, Pennsylvania, 2006.
- [8] Julie Kamm and James G. Nagy. Kronecker product and SVD approximations in image restoration. *Linear algebra and its applications*, 284(1-3):177–192, 1998.
- [9] Julie Kamm and James G. Nagy. Optimal Kronecker product approximation of block Toeplitz matrices. *SIAM Journal on Matrix Analysis and Applications*, 22(1):155–172, 2000.

- [10] Misha E. Kilmer, Karan Braman, and Ning Hao. Third order tensors as operators on matrices: A theoretical and computational framework with applications in imaging. *SIAM Journal on Matrix Analysis and Applications*, 34:148–172, 2013.
- [11] Misha E. Kilmer and James G. Nagy. Kronecker product approximations for dense block Toeplitz-plus-Hankel matrices. *Numerical Linear Algebra with Applications*, 14:581–602, 2007.
- [12] Misha E. Kilmer and Arvind K. Saibaba. Structured matrix approximations via tensor decompositions. *SIAM Journal on Matrix Analysis and Applications*, 43(4):1599–1626, 2022.
- [13] Tamara G. Kolda and Brett W. Bader. Tensor decompositions and applications. *SIAM review*, 51(3):455–500, 2009.
- [14] Charles F. Van Loan. The ubiquitous Kronecker product. *Journal of Computational and Applied Mathematics*, 123(1):85–100, 2000. Numerical Analysis 2000. Vol. III: Linear Algebra.
- [15] Charles Van Loan and Nikos P. Pitsianis. Approximation with Kronecker products. Technical report, Cornell University, 1992.
- [16] Jan R Magnus and Heinz Neudecker. The commutation matrix: some properties and applications. *The annals of statistics*, 7(2):381–394, 1979.
- [17] James G. Nagy. Decomposition of block Toeplitz matrices into a sum of Kronecker products with applications in image restoration. Technical report, Southern Methodist University, 1996.
- [18] James G. Nagy, Michael K. Ng, and Lisa Perrone. Kronecker product approximations for image restoration with reflexive boundary conditions. *SIAM Journal on Matrix Analysis and Applications*, 25(3):829–841, 2003.
- [19] Nikos P. Pitsianis. *The Kronecker product in approximation and fast transform generation*. Cornell University, 1997.
- [20] Eugene Tyrtyshnikov. Kronecker-product approximations for some function-related matrices. *Linear Algebra and its Applications*, 397:423–437, 2004.